Chapter 2

Statistical analysis of randomness

2.1 Introduction

Randomness in a light field is an inevitable and widespread phenomenon, often arising from erratic fluctuations in the light source or propagation of light through a random scattering media. When coherent light propagates through such random media, its wavefront becomes distorted, scrambling the light information. This process further aggravates coherent noise due to stochastic interference of randomly scattered waves, resulting in speckles and high-contrast, fine-scale granular patterns with well-defined statistical properties [4,140,226,227].

Since the invention of the laser in the early 1960s, speckle patterns have been treated as a nuisance in coherent optical imaging applications. However, these random fluctuations carry essential signatures of the light source and its propagating medium, which can be exploited for the analysis of the light source. A statistical treatment becomes important because of the difficulty associated with observing deterministic light propagation in the random scattering medium. Goodman and Dainty pioneered the statistical analysis of speckle patterns by studying speckles generated through the illumination of a monochromatic light source on a diffuser [140,226]. These statistical properties associated with the speckle field play a central role in determining the coherence and polarization properties of the randomly fluctuating field. For optical speckle patterns, measuring the correlation between speckle patterns at different space-time points is possible. These correlations provide insight into the statistical properties, such as the coherence and polarization of stochastic light fields [168].

Customizing the statistical properties of optical speckles has been a topic of considerable interest for a long time in the realm of physical and applied optics for decades [228–236]. While much of the focus has been on treating stochastic fields as scalar fields, the

vectorial nature of electromagnetic fields, i.e. polarization, has continued to attract attention for both fundamental and applied research [3,25,27,168,197,237–241]. The state of polarization (SOP) of a light field is typically described by the four Stokes parameters (SPs) and is visualized through polarization ellipses or the Poincaré sphere [27]. Experimental determination of the SOP of the light field is achievable using an interferometric [28,139] or non-interferometric [119,242] approach. Increasing interest in the polarization properties of speckles presented in terms of SPs has opened new research avenues for statistically characterizing the inherent randomness in stochastic fields [243–253].

However, the SOP of the light field may exhibit fluctuations in time and space. Characterization of these fluctuations provides useful statistical information about the source or propagating medium. The study of polarization dynamics and the evolution of the instantaneous SOP of an optical field have emerged as a key area of research for both fundamental understanding and practical applications. Measuring these dynamics offers insights into the characteristics of the light source and scattering medium [254–259]. Analysis of SOP fluctuation is relevant in diverse applications such as in optical communication [260], encompassing the investigation of polarization scattering within optical fibers [261], remote sensing [262], depolarization processes on rough surfaces or within disordered and complex media [263], diagnosis of samples of biological tissues [264], and the broader realm of biomedical applications [265–267], etc. Moreover, statistical properties of the polarization speckle play a crucial role in improving the image quality, widening the field of view [216], and in unconventional holography with unpolarized light [238,268].

The SOP of an arbitrary light source has random fluctuations in the phase and amplitude of the electric field. Thus, it is necessary to consider the temporal correlations between

those random variables to analyze the polarization dynamics properly. The temporal polarization dynamics of the electromagnetic beam have been demonstrated by determining polarization time, which allows an understanding of the random nature of polarization as a dynamic process in the Poincaré sphere [269]. Although polarization dynamics represent a characteristic of the fluctuations of the SOP of a light source, observation of instantaneous SOPs of natural thermal light is practically difficult as the detector's response time is slow compared to the fast fluctuations of light. Nevertheless, a slowly fluctuating Gaussian random field can be realized in the laboratory by illuminating a slowly rotating ground glass with a coherent light source. Propagation of coherent polarized light through a static scatterer introduces a spatial fluctuation in the SOP. The randomly scattered field is free from temporal fluctuation because the light is monochromatic, and the scatterer is static. It stays to be fully polarized according to the conventional definition based on temporal averaging. Such a coherent random field, with a well-defined and spatially fluctuating SOP at each point, is termed as a polarization speckle [189,191,211]. Polarization speckles exhibit spatially fluctuating, random polarization distribution. The precise morphology of the polarization speckle pattern is a deterministic signature of the light’s state of polarization fluctuation within a scattering medium. Given the inherent randomness of polarization speckle patterns, a statistical approach emerges as the most pragmatic method for their analysis.

For the polarization speckle, the statistical distribution of the SPs on the Poincaré sphere captures polarization fluctuation. Spatial fluctuations of polarization speckles play a vital role in biomedical imaging to deduce a large amount of information about the scale sizes (coarseness) of polarization speckles and the physical properties of a measured sample, such as dichroism and birefringence, and also in a variety of practical applications such as in speckle based imaging, diagnosis of scatterers, etc. [214,222]. The polarization

speckle field is fully polarized at any given time t according to the definition relying on temporal averaging of SPs. In contrast, the spatial degree of polarization (SDOP) based on the space averaging of SPs gives different values based on the randomness in spatially fluctuating polarization states [225,270].

Spatial averages can replace ensemble averages under the assumptions of ergodicity in space in certain cases. For a speckle field with a particular SDOP, the polarization state may change from one spatial point to another throughout the speckle pattern, and these random polarization fluctuations can be visualized graphically on the Poincaré sphere. Also, this random dynamic process can be treated with directional statistics, which is useful for modeling the polarization of stationary light sources by using a suitable probability density function (PDF) distribution on Poincaré sphere. Among them, the PDF of the vMF distribution, which has rotational symmetry and thus a circular probability contour, can be used to statistically study the dynamics of polarized, partially polarized, and unpolarized light sources on the Poincaré sphere [271]. The vMF distribution on the Poincaré sphere can be conceptualized to specify the spatial evolution of the polarization state of the spatially fluctuating random fields. However, such quantitative evaluation does not seem to exist for the polarization speckle despite its known fundamental and practical importance.

On the other hand, the seminal work by Emil Wolf on the wave nature of coherence paves the way for the characterization of stochastic fields such as laser speckle. A deeper understanding of two-point correlations can provide a significant tool for analyzing the statistical properties of speckle fields. Traditionally, two-point correlations are evaluated by the fringe visibility of interference patterns, and such a definition is generalized to include the vectorial nature of the light [194,195,272]. A compact portrayal of the coherence and polarization is possible with the aid of the coherence (two-point) SPs

[273]. The Poincaré sphere of electromagnetic spatial coherence has recently been introduced in random vectorial fields [274,275]. Additionally, multi-scale degree of polarization (MDOP), complex degree of mutual polarization (CDMP), etc., have been used to characterize polarization speckles and trace their physical origins by using autocorrelation of the CDMP [196,276,277].

Moreover, polarization dynamics can be evaluated by estimating the similarity of polarization states at two points by utilizing polarization correlation. The evolution of polarization in time and temporal polarization dynamics of the stationary electromagnetic beam has been implemented using the polarization correlations [278,279]. However, such a study has not attracted much attention to characterize spatial polarization dynamics of the speckle field except for a study using a polarization interferometer [280]. In this context, Singh et. al. have demonstrated the characterization of spatial polarization fluctuation of polarization speckle using correlation of orthogonally polarized speckle fields and extended the concept of polarization length to the spatial domain [280].

In this chapter, we explore statistical characterization methods for statistically analyzing different types of polarization speckles and demonstrate two novel experimental techniques, which will be discussed in the coming sections.

2.2 vMF distribution on the Poincaré Sphere

In the first technique, we experimentally measured the statistical signature of the polarization speckle using vMF distribution on the Poincaré sphere. At first, we discuss the prime outlines of mathematical and physical illustrations to characterize polarization information of the speckle field using statistics of random SPs. We utilize the vMF distribution on the Poincaré sphere to provide statistical insights into the spatial evolution of the polarization state of the polarization speckle. The behavior of the marginal vMF

distribution on the axes of the Poincaré sphere and its association with the analytically evaluated PDF of the normalized Stokes parameter (NSPs) of the polarization speckle are examined. This allows us to reveal the connection between the SDOP and averaged NSPs with the spatial concentration parameter and spatial mean direction. For experimental verification and testing of the theoretical basis, a specially designed interferometry setup is used for single-shot detection of Stokes parameters (SPs) and NSPs of the polarization speckles. Statistical analysis of the polarization speckles with the theoretical basis is tested on the experimental results, and a similar analysis is conducted on the simulated results. We found a good agreement between analytical PDF and experimental/simulation results, demonstrating our approach's usefulness for analyzing the spatially fluctuating polarization. Detailed theoretical framework, numerical simulation, and experimental results are discussed below.

2.2.1 Theoretical details

Consider a transversely polarized monochromatic field with the orthogonal axes *x* and *y* propagating along the *z* direction. The instantaneous representation of the complex field at a distance *z* and at an instant of time *t* can be expressed as

$$\boldsymbol{U}\left(\boldsymbol{r},t\right)=U_x\left(\boldsymbol{r},t\right)\hat{e}_x+U_y\left(\boldsymbol{r},t\right)\hat{e}_y, \tag{2.1}$$

where $U_x\left(\boldsymbol{r},t\right)$ and $U_y\left(\boldsymbol{r},t\right)$ are the orthogonal polarization components of the field, $\boldsymbol{r}$ is the spatial position vector, and $\hat{e}_x$ and $\hat{e}_y$ denotes the horizontal and vertical polarization states of the light, respectively.

Orthogonal polarization components of the complex field are represented as,

$$U_x\left(\boldsymbol{r},t\right)=U_x^{re}\left(\boldsymbol{r},t\right)+iU_x^{im}\left(\boldsymbol{r},t\right)=A_x\left(\boldsymbol{r},t\right)\exp\left(i\alpha_x\left(\boldsymbol{r},t\right)\right),$$

$$U_y(\boldsymbol{r},t) = U_y^{re}(\boldsymbol{r},t) + iU_y^{im}(\boldsymbol{r},t) = A_y(\boldsymbol{r},t)\exp\left(i\alpha_y(\boldsymbol{r},t)\right), \tag{2.2}$$

with superscripts '*re*' and '*im*' representing real and imaginary parts and $A_x, A_y, \alpha_x, \alpha_y$ representing amplitudes and phases respectively with relative phase, $\alpha = \alpha_y - \alpha_x$. For convenience, we ignored time *t* for further calculations.

The SPs for the spatially fluctuating coherent fields, as represented in Eq. (2.1), are defined as [27],

$$\begin{aligned} S_m(\boldsymbol{r}) &= \boldsymbol{U}^{\dagger}(\boldsymbol{r})\boldsymbol{\sigma}^m\boldsymbol{U}(\boldsymbol{r}), \qquad (m=0,1,2,3), \\ &= \sum_{a,b}\sigma_{ab}^m U_a^*(\boldsymbol{r})U_b(\boldsymbol{r}), \quad (a,b=\mathrm{x},\mathrm{y}), \end{aligned} \tag{2.3}$$

where † , * denotes the Hermitian conjugate, complex conjugate respectively, $\boldsymbol{\sigma}^0, \boldsymbol{\sigma}^1, \boldsymbol{\sigma}^2, \boldsymbol{\sigma}^3$ are the 2×2 identity matrix and three Pauli spin matrices respectively.

To extract statistics of polarization speckle on the Poincaré sphere, we introduce NSPs as,

$$\tilde{S}_m(\boldsymbol{r}) = \frac{S_m(\boldsymbol{r})}{S_0(\boldsymbol{r})}, \tag{2.4}$$

The NSPs emphasize the SOP at a particular point and can be graphically represented by a point on or inside the Poincaré sphere.

To evaluate the spatial inhomogeneity of the random field, we use the SDOP [191] as,

$$P_s^2(\boldsymbol{r}) = \left(\omega_1^s(\boldsymbol{r})\right)^2 + \left(\omega_2^s(\boldsymbol{r})\right)^2 + \left(\omega_3^s(\boldsymbol{r})\right)^2, \tag{2.5}$$

where the averaged NSPs are introduced as,

$$\omega_1^s(\boldsymbol{r}) = \left\langle \tilde{S}_1(\boldsymbol{r}) \right\rangle,$$

$$\omega_2^s(\boldsymbol{r}) = \left\langle \tilde{S}_2(\boldsymbol{r}) \right\rangle,$$

$$\omega_3^s(\boldsymbol{r}) = \left\langle \tilde{S}_3(\boldsymbol{r}) \right\rangle, \tag{2.6}$$

with $\langle\ \rangle$ representing spatial averaging.

The value of the SDOP lies between 0 and 1, $P_s=1$ for a spatially fully polarized, $P_s=0$ for a spatially unpolarized and $0<P_s<1$ for a spatially partially polarized light field. P_s measures spatial inhomogeneity of polarization distribution of the speckle but does not specify the polarization dynamics.

For the Gaussian statistics, the joint PDF of the field variables depends on the correlation of four components $U_x^{re}, U_x^{im}, U_y^{re}, U_y^{im}$ of the field and is given as [281],

$$P\left(U_x^{re}, U_x^{im}, U_y^{re}, U_y^{im}\right) = \frac{1}{\pi^2 |J|} \exp\left[-\frac{1}{|J|}\left(J_{yy} U_x^* U_x + J_{xx} U_y^* U_y - 2\,\mathrm{Re}(J_{xy} U_x^* U_y) \right) \right], \tag{2.7}$$

Where, $|J|$ is the determinant of the 2x2 polarization matrix $\boldsymbol{J}$, represented as [5],

$$\boldsymbol{J}(\boldsymbol{r},\boldsymbol{r}) = \begin{bmatrix} J_{xx}(\boldsymbol{r},\boldsymbol{r}) & J_{xy}(\boldsymbol{r},\boldsymbol{r}) \\ J_{yx}(\boldsymbol{r},\boldsymbol{r}) & J_{yy}(\boldsymbol{r},\boldsymbol{r}) \end{bmatrix}, \tag{2.8}$$

where, $J_{ab}(\boldsymbol{r},\boldsymbol{r}) = \left\langle U_a^*(\boldsymbol{r}) U_b(\boldsymbol{r}) \right\rangle$ is the elements of the polarization matrix, $\boldsymbol{J}(\boldsymbol{r},\boldsymbol{r})$.

Transforming field variables to amplitude and phase as in Eq. (2.2), the joint PDF of amplitude and relative phase is given by

$$P\left(A_x, A_y, \alpha\right) = \frac{1}{\pi^2 \left|J\right|} \int_0^\infty r_1 r_2 dr_1 dr_2 \int_0^{2\pi} d\theta_1 d\theta_2 \delta\left[\alpha - \left(\theta_2 - \theta_1\right)\right] \delta\left(A_x - r_1\right) \delta\left(A_y - r_2\right)$$

$$\times \exp\left[-\frac{1}{\left|J\right|} \left(J_{yy} r_1^2 + J_{xx} r_2^2 - 2\left|J_{xy}\right| r_1 r_2 \cos\left(\theta_2 - \theta_1 - \gamma\right)\right)\right],$$

$$= \frac{2\pi - \alpha}{\pi^2 \left|J\right|} A_x A_y \exp\left[-\frac{1}{\left|J\right|} \left(J_{yy} I_x + J_{xx} I_y - 2\left|J_{xy}\right| A_x A_y \cos\left(\alpha - \gamma\right)\right)\right]. \tag{2.9}$$

where, $\gamma = \arg\left(J_{xy}\right)$, and $r_1, r_2, \theta_1, \theta_2$ are the amplitude and phase variables used for the integration performed for the coordinate transformation from field variables to amplitude and phase variables.

The joint PDF of amplitude variables by integrating out the phase variable α is given as,

$$P\left(A_x, A_y\right) = \frac{2\pi - \alpha}{\pi \left|J\right|} A_x A_y \exp\left[-\frac{1}{\left|J\right|} \left(J_{yy} I_x + J_{xx} I_y \right)\right] \frac{1}{\pi} \int_0^{2\pi} \exp\left[\frac{2}{\left|J\right|} \left|J_{xy}\right| A_x A_y \cos\left(\alpha - \gamma\right)\right] d\alpha,$$

$$= \frac{2\left(2\pi - \alpha\right)}{\pi \left|J\right|} A_x A_y \exp\left[-\frac{1}{\left|J\right|} \left(J_{yy} I_x + J_{xx} I_y \right)\right] I_0\left(\frac{2}{\left|J\right|} \left|J_{xy}\right| A_x A_y \right), \tag{2.10}$$

where, $I_0\left(\ldots\right)$ is the modified Bessel function of the first kind of order zero.

A joint PDF of the intensity variables is given by [282]

$$P_{I_x, I_y}\left(I_x, I_y\right) = \frac{4}{S_0{}^2 \left(1 - P_s^2\right)} \exp\left[-\frac{2}{S_0 \left(1 - P_s^2\right)} \left\{ \left(I_x + I_y\right) + \left(I_y - I_x\right) \omega_1^s \right\}\right] I_0\left(\frac{4\sqrt{P_s^2 - \omega_1^{s2}}}{S_0 \left(1 - P_s^2\right)} \sqrt{I_x I_y} \right),$$

(2.11)

Setting an auxiliary variable, $v \equiv I_y \big/ I_x$ we obtain

$$P_v\left(v\right) = \int I_x P_{I_x, I_y}\left(I_x, v I_x\right) dI_x,$$

$$= \frac{4}{S_0{}^2\left(1-P_s^2\right)} \int I_x \exp\left[-\frac{2}{S_0\left(1-P_s^2\right)} \left\{ \left(I_x + vI_x\right) + \left(vI_x - I_x\right)\omega_1^s \right\} \right] I_0\left(\frac{4\sqrt{P_s^2 - \omega_1^{s2}}}{S_0\left(1-P_s^2\right)} \sqrt{I_x . vI_x} \right) dI_x \qquad (2.12)$$

Employing the known integral, $\int_0^\infty k \exp\left(-pk\right) I_0\left(ak\right) dk = \frac{p}{\left(p^2 - a^2\right)^{3/2}}$, Eq. (2.12) transforms to

$$P_v\left(v\right) = \frac{\left(1-P_s^2\right)\left[\left(1+v\right) + \left(v-1\right)\omega_1^s\right]}{\left[\left\{\left(1+v\right) + \left(v-1\right)\omega_1^s\right\}^2 - 4v\left(P_s^2 - (\omega_1^s)^2\right)\right]^{3/2}}. \qquad (2.13)$$

PDF of another auxiliary variable $V \equiv \frac{1-v}{1+v} = f\left(v\right)$ can be expressed as

$$P_U\left(V\right) = \frac{P_v\left(f^{-1}\left(V\right)\right)}{\left|\frac{dV}{dv}\right|}. \qquad (2.14)$$

From Eq. (2.4), one of the NSPs can be written as

$$\tilde{S}_1\left(\boldsymbol{r}\right) = \frac{I_x - I_y}{I_x + I_y} = \frac{1 - \frac{I_y}{I_x}}{1 + \frac{I_y}{I_x}}. \qquad (2.15)$$

Eq. (2.14) is transformed to,

$$P_{\tilde{S}_1}\left(\tilde{S}_1\right) = \frac{2}{\left(1+\tilde{S}_1\right)^2} P_v\left(\frac{1-\tilde{S}_1}{1+\tilde{S}_1}\right). \qquad (2.16)$$

To evaluate the above expression, we calculate

$$P_v\left(\frac{1-\tilde{S}_1}{1+\tilde{S}_1}\right)=\frac{\left(1-P_s^2\right)\left[\left(1+\frac{1-\tilde{S}_1}{1+\tilde{S}_1}\right)+\left(\frac{1-\tilde{S}_1}{1+\tilde{S}_1}-1\right)\omega_1^s\right]}{\left[\left\{\left(1+\frac{1-\tilde{S}_1}{1+\tilde{S}_1}\right)+\left(\frac{1-\tilde{S}_1}{1+\tilde{S}_1}-1\right)\omega_1^s\right\}^2-4\frac{1-\tilde{S}_1}{1+\tilde{S}_1}\left(P_s^2-\left(\omega_1^s\right)^2\right)\right]^{3/2}},$$

$$=\frac{\left(1-P_s^2\right)\left(1-\tilde{S}_1\omega_1^s\right)\left(1+\tilde{S}_1\right)^2}{4\left[\left(1-\tilde{S}_1\omega_1^s\right)^2-\left(1-\left(\tilde{S}_1\right)^2\right)\left(P_s^2-\left(\omega_1^s\right)^2\right)\right]^{3/2}}. \tag{2.17}$$

Now, from Eq. (2.17) using Eq. (2.16), we obtain an expression for the PDF of NSP, $\tilde{S}_1$, which is given by,

$$\mathrm{P}_{\tilde{S}_1}\left(\tilde{S}_1\right)=\frac{\left(1-P_s^2\right)}{2}\frac{\left(1-\tilde{S}_1\omega_1^s\right)}{\left[\left(1-\tilde{S}_1\omega_1^s\right)^2-\left(1-\left(\tilde{S}_1\right)^2\right)\left(P_s^2-\left(\omega_1^s\right)^2\right)\right]^{3/2}}. \tag{2.18}$$

Similarly, PDFs of NSPs $\tilde{S}_2,\tilde{S}_3$ are given as,

$$\mathrm{P}_{\tilde{S}_2}\left(\tilde{S}_2\right)=\frac{\left(1-P_s^2\right)}{2}\frac{\left(1-\tilde{S}_2\omega_2^s\right)}{\left[\left(1-\tilde{S}_2\omega_2^s\right)^2-\left(1-\left(\tilde{S}_2\right)^2\right)\left(P_s^2-\left(\omega_2^s\right)^2\right)\right]^{3/2}}, \tag{2.19}$$

$$\mathrm{P}_{\tilde{S}_3}\left(\tilde{S}_3\right)=\frac{\left(1-P_s^2\right)}{2}\frac{\left(1-\tilde{S}_3\omega_3^s\right)}{\left[\left(1-\tilde{S}_3\omega_3^s\right)^2-\left(1-\left(\tilde{S}_3\right)^2\right)\left(P_s^2-\left(\omega_3^s\right)^2\right)\right]^{3/2}}. \tag{2.20}$$

The vMF distribution is used to model data lying on the unit sphere's surface. The joint PDF of vMF distribution for a random unit vector of the NSPs, $\tilde{S}\left(\tilde{S}_1,\tilde{S}_2,\tilde{S}_3\right)$ is given by [283,284],

$$f\left(\tilde{S};\mu^s,\kappa_s\right)=\frac{\kappa_s}{4\pi\ Sinh\,\kappa_s}e^{\kappa_s\left(\mu^s\right)^T\tilde{S}}\qquad \kappa_s\geq 0, \tag{2.21}$$

where, $\mu^s = \left(\mu_1^s, \mu_2^s, \mu_3^s\right)$ is the spatial mean direction and κ_s is the spatial concentration parameter. Polarization distribution is clustered around the spatial mean direction, μ^s. The spatial concentration parameter measures whether the polarization distribution is spatially more uniform or random. For larger values of the spatial concentration parameter, the polarization distribution is more uniform, while for smaller values, it is more sparsely distributed. PDF of NSPs as described in Eqs. (2.18-2.20) can be related to the marginal vMF distribution on the axes of the Poincaré sphere. The relation between averaged NSPs and spatial mean direction is given by [284],

$$\omega^s = \left(coth\kappa_s - \frac{1}{\kappa_s} \right) \mu^s. \tag{2.22}$$

This allows us to find out the relation between the SDOP and spatial concentration parameters as

$$P_s = coth\kappa_s - \frac{1}{\kappa_s}. \tag{2.23}$$

For $\kappa_s \to 0$, P_s is zero, which signifies a spatially unpolarized speckle pattern. The vMF distribution of Eq. (2.21) gives value $f\left(\tilde{S}; \mu^s, 0\right) = \frac{1}{4\pi}$, and states that all the SOP of the polarization speckles on the Poincaré sphere are equally probable for $\kappa_s \to 0$. For $\kappa_s \to \infty$, polarization is same over the speckle pattern and vMF distribution of Eq. (2.21) tends to Dirac distribution $f\left(\tilde{S}; \mu^s, \infty\right) = \delta\left(\tilde{S} - \mu^s\right)$. This represents a single point on the Poincaré sphere which corresponds to the same polarization state over the speckle pattern.

Equation (2.18-2.23) are our main results in this technique [284], and are utilized for the statistical analysis of polarization speckle.

2.2.2 Experiment

To illustrate the feasibility of the proposed technique and analyze the statistical properties of polarization speckles, we used an experimental setup to generate the polarization speckle and simultaneously measure both the orthogonal polarization components of the random light field at a fixed time *t*. Measurement of the complex fields of the polarization component is implemented by a field-based polarization interferometer as shown in Fig. 2.1. A detailed description of the experimental procedure is as follows. The light beam of wavelength 632.8nm from a linearly polarized He-Ne Laser (Thorlabs, HNL150L) is converted into 45° linearly polarized by a half-wave plate (HWP1). The beam is spatially filtered using a combination of a microscopic objective (MO), a pinhole (P), and a collimated lens (L1). The collimated beam splits by a beam splitter (BS1) into two arms of the interferometer. A beam transmitted by the BS1 enters into a specially designed triangular Sagnac interferometer, creating two mutually tilted orthogonally polarized reference beams at the detector plane. A diagonally polarized beam splits into two orthogonal polarization components by a PBS1 (Thorlabs, PBS25-633). It is directed in opposite directions and focused at two different locations at the back focal plane of lens L3 by mirrors M1 and M2 (Thorlabs, PF10-03-G01). This strategy helps to achieve distinguishable linear phases and tilts into the orthogonally polarized reference beams at the back focal plane of lens L2, as shown in Fig. 2.1. Appropriate amounts of tilts to the orthogonally polarized beams create a spatial-frequency-multiplexed carrier fringe suitable for Fourier fringe analysis. On the other hand, a beam reflected from the BS1 enters into a triangular Sagnac geometry composed of a PBS2 and mirrors M3 and M4. This geometry is used to generate polarization speckles and control their statistics. We create two replicas of the source and their separation at the ground glass (GG) (Thorlabs, DG20-120-MD) plane is controlled by the triangular Sagnac geometry as described in

Fig. 2.2. A circular aperture (CA) is imaged through the Sagnac geometry by lens L4 in such a way that two counter-propagating beams together generate two copies of the aperture on the GG plane. Separation between these two copies at the GG can be controlled by shifting mirrors M3 and M4.

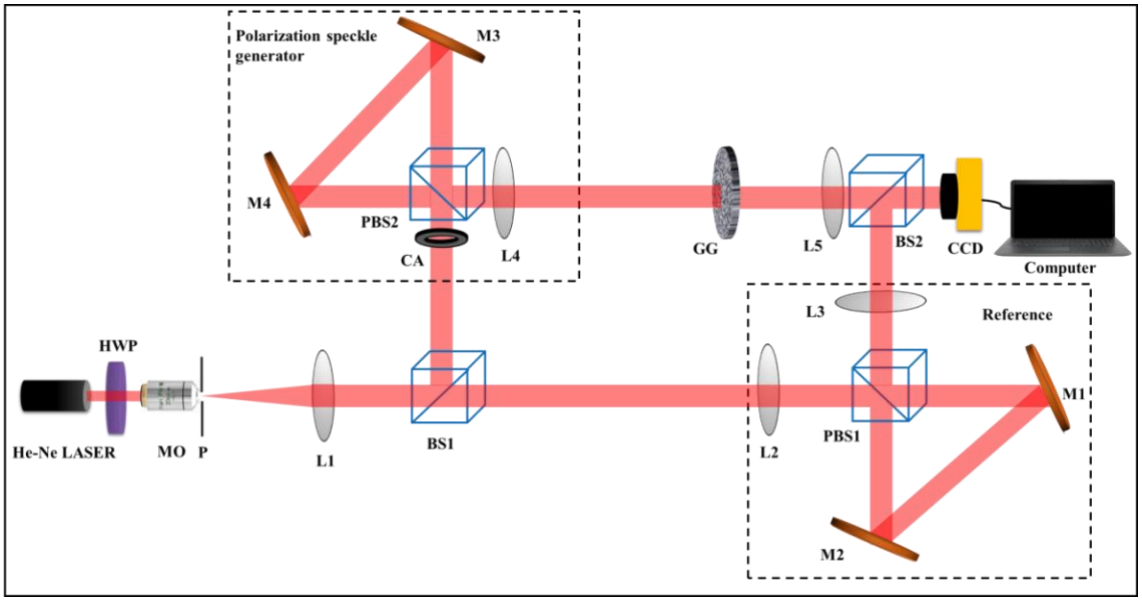

Fig. 2.1 Experimental setup for polarization speckle for different degrees of spatial polarization fluctuation. Laser: He-Ne laser; MO: Microscope objective; P: Pinhole; HWP: Half-wave plate; BS1, BS2: Beam splitters; PBS1, PBS2: Polarization Beam Splitters; M1, M2, M3, M4: Mirrors; L1, L2, L3, L4, L5: Lenses; GG: Ground glass; CA: Circular Aperture; CCD: Charge-coupled device; Computer.

Three different polarization speckles are considered due to the overlap of the orthogonally polarized sources at the GG plane. A full overlap of the orthogonally polarized sources on the GG plane represents a case where the speckle field is uniformly polarized. The second case represents a situation where a polarization speckle is generated by the partial overlap of the orthogonally polarized sources at the GG plane. The third case represents a speckle pattern due to fully separated orthogonally polarized sources at the GG plane. The random field at the plane GG is Fourier transformed at the detector plane by a lens L5.

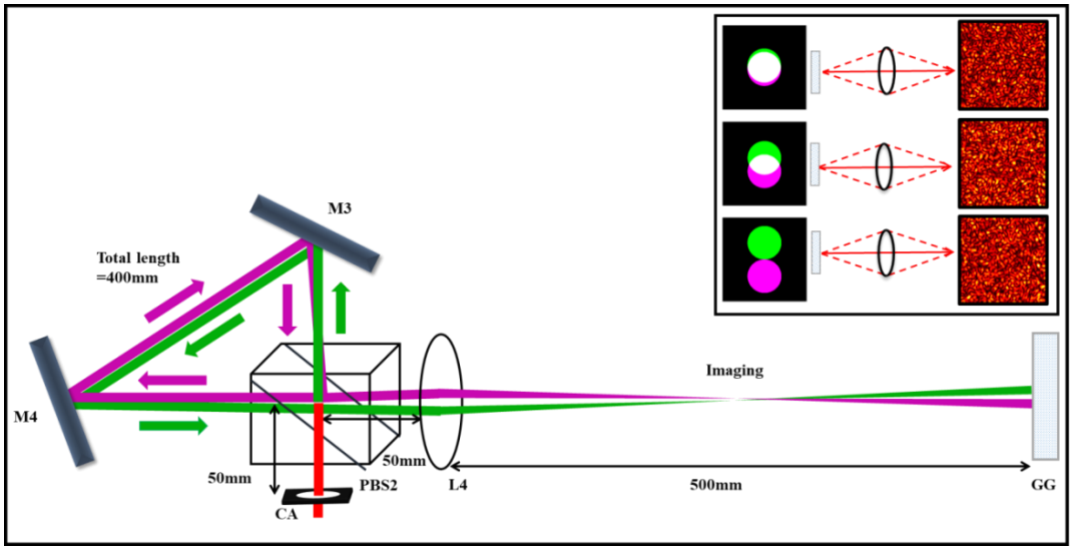

Fig. 2.2 Detailed view of Sagnac geometry for imaging and controlling the overlap of two orthogonally polarized light fields on the ground glass. A red color represents incident diagonally polarized light. Green and pink colors represent two orthogonally polarized light fields, and white color represents the overlapping area of two orthogonally polarized light fields. The inset shows experimental geometry for creating three different cases of polarization speckle.

The scattered field from the GG interferes with the reference beam at the Fourier plane of lens L5, and the randomly scattered orthogonal polarization components encoded in the interference pattern are recorded by a charge-coupled device (CCD) with a pixel size of 7.4μm. The Fourier fringe analysis of the polarization multiplexed interferogram permits simultaneous recovery of the randomly scattered orthogonal polarization components. While recording, we considered speckle grains bigger than CCD pixel size. The experimentally retrieved complex field components are used to obtain all four SPs and NSPs using Eq. (2.3) and (2.4), which are used to plot vMF distribution on the Poincaré sphere. Digital evaluations of the spatial average of NSPs are performed as in Eq. (2.6) to evaluate the SDOP of Eq. (2.5). Following these data, using Eq. (2.18-2.20), PDFs of NSPs, $\tilde{S}_1, \tilde{S}_2, \tilde{S}_3$ as well as marginal PDF of vMF distribution are obtained for the experimental demonstrations. Also, the spatial mean direction and concentration parameters are calculated using Eq. (2.22), (2.23).

2.2.3 Results and discussions

Structured polarization speckles with the desired statistical features are obtained by overlapping two mutually orthogonal circular sources of diameter 4mm at the GG plane. Random scattering of three different cases of polarized sources is schematized in the inset of Fig. 2.2 on the right-hand side. To test a developed theoretical basis and compare with the experimental results, simulations of three different polarization speckles are covered as explained in the inset of Fig. 2.2. Simulation of the polarization speckle is realized by modeling the two coherent orthogonally polarized light fields with a circular size of diameter 4mm and at a wavelength 632.8 nm. A GG is considered to insert a uniform random phase distribution in the range of $[-\pi,\pi]$ in the incoming light, and randomly scattered light propagation from the source to the observation plane is modeled using a discrete fast Fourier transform. Three different source structures are modeled by controlling the separation between two orthogonally polarized lights at the GG plane. Hence, a polarization fluctuating random field is generated due to contributions from two orthogonally polarized and coherent random sources. As explained in the theory section, a statistical analysis of simulated polarization speckles is performed to observe spatial polarization fluctuations using the vMF distribution on the Poincaré sphere.

A set of experimentally measured complex field's amplitude distributions of horizontally and vertically polarized components of polarization speckles $(U_x(\boldsymbol{r}),U_y(\boldsymbol{r}))$ are shown in Fig. 2.3 for three different cases. These complex fields allow us to measure all four SPs of polarization speckles and NSPs from the single-shot intensity frame using Eq. (2.3) and (2.4). Considering spatial stationarity at the observation plane, we replaced the ensemble average with the spatial average over the image sensing area of CCD to obtain averaged NSPs and simultaneously SDOP for the three different cases of the polarization speckle.

Simulation and experimental results of the averaged NSPs, and SDOPs are summarized in Table 2.1.

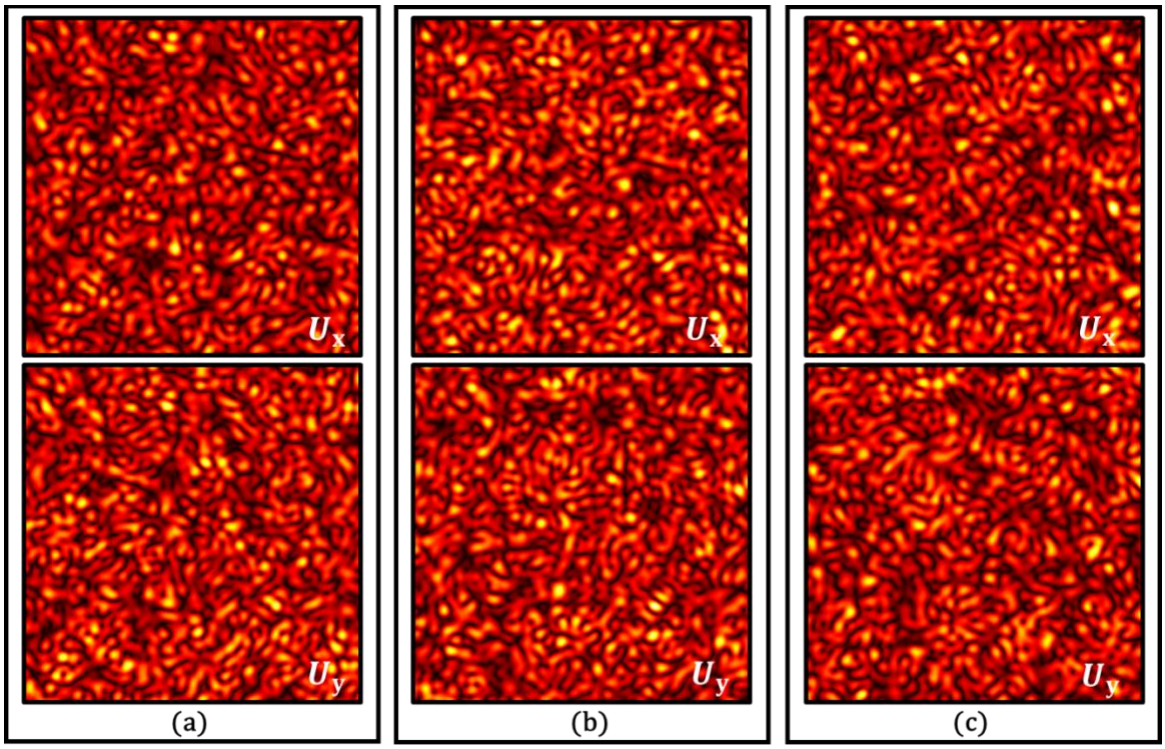

Fig. 2.3 Experimentally measured amplitude distribution of horizontal and vertically polarized scattered fields at the CCD plane for three different cases of polarization speckle: (a) full overlap, (b) partial overlap, and (c) full separation.

The simulation result of the joint PDF of the vMF distribution on the Poincaré sphere is shown in Fig. 2.4(a) for a fully overlapping case. Histograms in Figs. 2.4(b)-(d) represent projections on the axes, of distribution points on the Poincaré sphere associated with the vMF distribution of the simulation result as shown in Fig. 2.4(a). Corresponding experimental results are shown in Figs. 2.4(e)-(h). Fig. 2.4(e) represents the joint PDF of the vMF distribution and histograms in Figs. 2.4(f)-(h) represent projections on the axes, of distribution points on the Poincaré sphere associated with the vMF distribution as shown in Fig. 2.4(e) for the experimental result of the fully overlapping case. A good match between the simulation and experimental results can be noticed from Figs. 2.4(a)-(d) and 2.4(e)–(h) respectively. The solid curves in Figs 2.4(b)-(d) for simulation and

2.4(f)-(h) for experiment, represent analytically evaluated PDF of NSPs $\tilde{S}_1, \tilde{S}_2, \tilde{S}_3$ by using Eq. (2.18), (2.19), and (2.20) with the known SDOPs and averaged NSPs as given in Table 2.1. Pink and blue colors indicate the analytically evaluated PDF of NSPs $\tilde{S}_1, \tilde{S}_2, \tilde{S}_3$ for the simulation and experimental results respectively. We see that the histograms show the same statistical behaviour as the PDF of NSPs $\tilde{S}_1, \tilde{S}_2, \tilde{S}_3$ for the fully overlapping case. Similarly, simulation results for the partially overlapped case are shown in Fig. 2.5(a)-(d) and corresponding experimental results are shown in Fig. 2.5(e)-(h).

	$(\omega_1^s, \omega_2^s, \omega_3^s)$		P_s	
Overlap	Simulation	Experiment	Simulation	Experiment
Fully overlapped	-0.0009,0.8384, 0.0039	-0.0316,0.8336, 0.0819	0.8384	0.8383
Partially overlapped	-0.0179,0.3808,-0.2020	0.0032,0.3520, -0.2612	0.4314	0.4389
Fully separated	-0.0639,0,0	-0.0389,0,0	0.0639	0.0389

Table 2.1 Simulation and experimental results of averaged NSPs, and SDOPs for three different types of overlap.

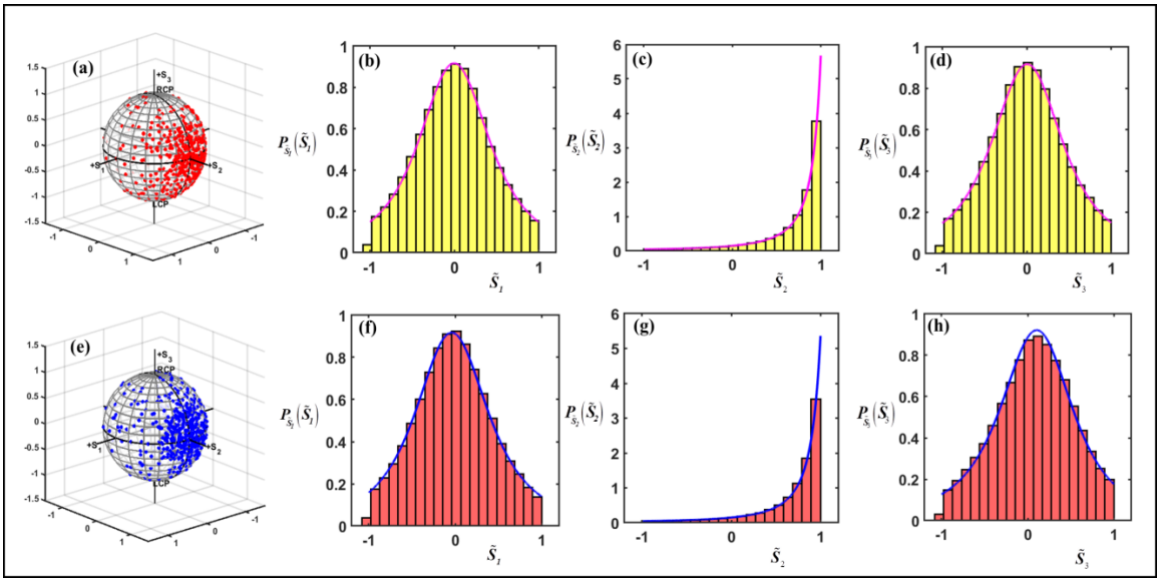

Fig. 2.4 The first row represents the simulation results for polarization speckle with a fully overlapping case: (a) a joint PDF of the vMF distribution on the Poincaré sphere. Histograms represent marginal vMF distribution on the axis of (b) $\tilde{S}_1$ (c) $\tilde{S}_2$ (d) $\tilde{S}_3$. Second row represents corresponding experimental results: (e) a joint PDF of the vMF distribution on the Poincaré sphere; histograms of the marginal vMF distribution on the axis of (f) $\tilde{S}_1$ (g) $\tilde{S}_2$ (h) $\tilde{S}_3$. Analytically evaluated PDF of NSPs $\tilde{S}_1, \tilde{S}_2, \tilde{S}_3$ is represented by pink and blue colors for simulation and experimental results in the first and second row respectively.

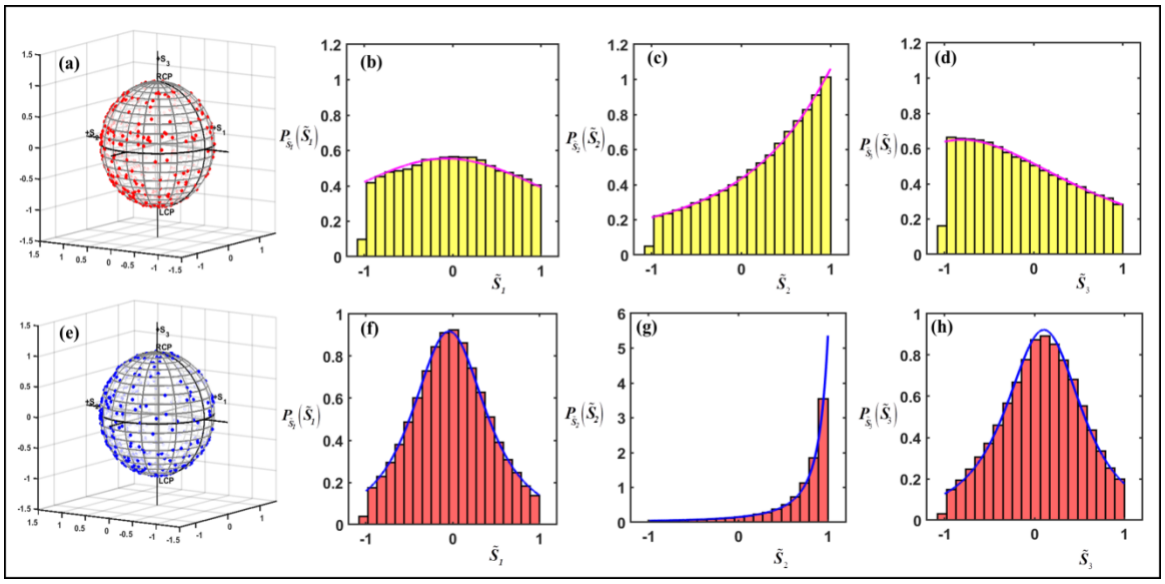

Fig. 2.5 The first row represents the simulation results for polarization speckle with a partially overlapping case: (a) a joint PDF of the vMF distribution on the Poincaré sphere. Histograms represent marginal vMF distribution on the axis of (b) $\tilde{S}_1$ (c) $\tilde{S}_2$ (d) $\tilde{S}_3$.

Second row represents corresponding experimental results: (e) a joint PDF of the vMF distribution on the Poincaré sphere; histograms of the marginal vMF distribution on the axis of (f) $\tilde{S}_1$ (g) $\tilde{S}_2$ (h) $\tilde{S}_3$. Analytically evaluated PDF of NSPs $\tilde{S}_1, \tilde{S}_2, \tilde{S}_3$ is represented by pink and blue colors for simulation and experimental results in the first and second row respectively.

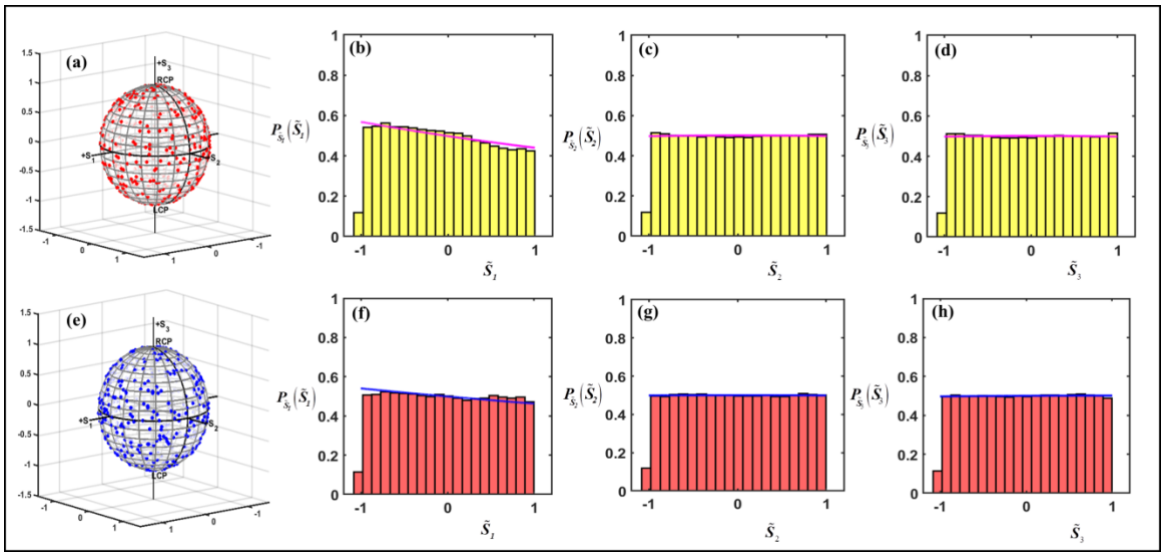

Fig. 2.6 The first row represents the simulation results for polarization speckle with a fully separated case: (a) a joint PDF of the vMF distribution on the Poincaré sphere. Histograms represent marginal vMF distribution on the axis of (b) $\tilde{S}_1$ (c) $\tilde{S}_2$ (d) $\tilde{S}_3$. Second row represents corresponding experimental results: (e) a joint PDF of the vMF distribution on the Poincaré sphere; histograms of the marginal vMF distribution on the axis of (f) $\tilde{S}_1$ (g) $\tilde{S}_2$ (h) $\tilde{S}_3$. Analytically evaluated PDF of NSPs $\tilde{S}_1, \tilde{S}_2, \tilde{S}_3$ is represented by pink and blue colors for simulation and experimental results in the first and second row respectively.

Simulation results for the fully separated case are shown in Fig. 2.6(a)-(d) and corresponding experimental results are shown in Fig. 2.6(e)-(h). In the partially overlapped and fully separated case also, the histograms show the same statistical behaviour as the PDF of NSPs $\tilde{S}_1, \tilde{S}_2, \tilde{S}_3$. So, the vMF distribution of NSPs is well adapted to the statistical analysis of spatial polarization distribution on the Poincaré sphere.

The inference drawn from the joint PDF plots of the vMF distribution on the Poincaré sphere, specifically depicted in Figs. 2.4(a,e), 2.5(a,e), and 2.6(a,e), reveals that transitioning from a fully overlapped to a fully separated scenario results in a more randomized spatial evolution of the state of polarization (SOP). This trend is distinctly visualized in the corresponding figures. From the experimental data, using Eq. (2.22), (2.23), we calculate the spatial mean direction and spatial concentration parameter for the three different cases which are shown in Table 2.2.

	$\left(\mu_1^s, \mu_2^s, \mu_3^s\right)$		κ_s	
Overlap	Simulation	Experiment	Simulation	Experiment
Fully overlapped	-0.0010,1,0.0046	-0.0377,0.994,0.0977	6.1878	6.1839
Partially overlapped	-0.0414,0.8827,-0.4682	-0.0073,0.8020,-0.5951	1.4701	1.5034
Fully separated	0,0,0	0,0,0	0.1921	0.1168

Table 2.2 Simulation and experimental results of spatial mean direction and spatial concentration parameter for three different types of overlap.

2.3 Poincaré vector correlations

In the second technique presented in this chapter, our goal is to demonstrate a new and stable experimental method, based on non-interferometry, to measure the SPs and estimate the spatial polarization dynamics of the polarization speckle. This is

implemented by using the correlations of the SPs at two spatial points (rather than temporal points). Out of the sixteen elements of the 4x4 correlation matrix of the Stokes parameters, we use only the diagonal elements to determine the polarization dynamics of the polarization speckle. For experimental tests of our method, we designed an experimental set-up for the controlled generation of three different categories of polarization speckles, and measurement of the SPs in the polarization speckles are carried out by using different orientations of a quarter wave plate and a polarizer in four shots. The experimental system in this paper is composed of two parts. The first part covers the synthesis of different polarization speckles for tests. The second part covers the non-interferometric experimental measurement of the SPs of the speckle. The proposed theoretical framework is also verified by simulation results and compared with the experimental results. We find good agreement between simulation and experimental results which confirms the accuracy and usefulness of our method. The detailed theoretical approach and corresponding experimental execution are discussed in the upcoming sections

2.3.1 Theoretical framework

For a two-dimensional (2D) orthogonally polarized light field propagating along the *z*-axis, the complex field and the SPs are expressed using Eq. 2.1 and 2.3, as described in previous section.

These four SPs are used to construct the Poincaré vector, which can be used to visualize the SOP on the Poincaré sphere. The Poincaré vector is represented as

$$\boldsymbol{S}(\boldsymbol{r}) = \left[S_1(\boldsymbol{r}), S_2(\boldsymbol{r}), S_3(\boldsymbol{r})\right] = \hat{\boldsymbol{s}}(\boldsymbol{r}) S_0(\boldsymbol{r}), \tag{2.24}$$

where the unit vector $\hat{s}(r)$ represents the SOP at a point r. Hence the Poincaré vector can be rendered as a product of the vector quantity $\hat{s}(r)$ and scalar quantity $S_0(r)$.

A diagrammatic representation of the space-time distribution of time-frozen polarization speckles is shown in Fig. 2.7. Instead of considering a temporally fluctuating random field along the time axis (*t*), we consider a time-frozen speckle pattern at a transverse plane as represented in Fig. 2.7. Our interest is to characterize such random field. The SOP changes as we move from observation point r_1 to r_2 due to a spatial fluctuation of the polarization. To observe the spatial polarization dynamics, the correlation of the Poincaré vector is used to provide details about how rapidly the SOP changes between two spatial points.

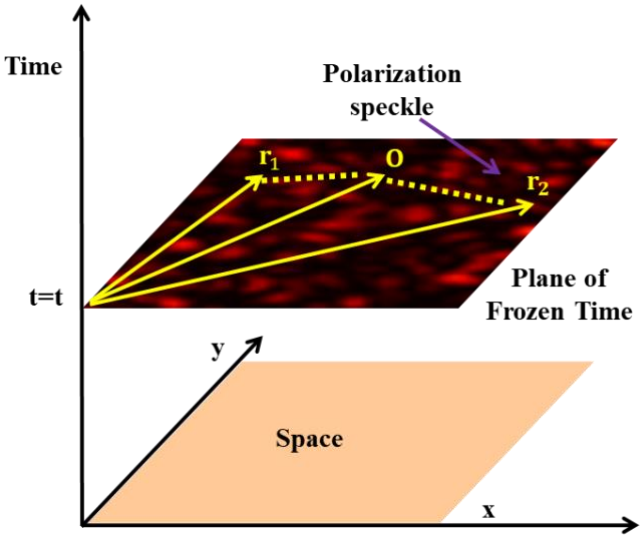

Fig. 2.7 Space-time distribution of polarization speckles. Points r_1 and r_2 with respect to a centre point 'O' represent two observation points in a time-frozen speckle.

The two-point correlations of SPs [280] are defined as

$$C_{mn}(r_1, r_2) = \langle S_m(r_1) S_n(r_2) \rangle \quad m, n = 0, 1, 2, 3, \tag{2.25}$$

which is represented by a 4x4 matrix as

$$C_{mn}(\boldsymbol{r_1},\boldsymbol{r_2}) = \begin{pmatrix} \langle S_0(\boldsymbol{r_1})S_0(\boldsymbol{r_2})\rangle & \langle S_0(\boldsymbol{r_1})S_1(\boldsymbol{r_2})\rangle & \langle S_0(\boldsymbol{r_1})S_2(\boldsymbol{r_2})\rangle & \langle S_0(\boldsymbol{r_1})S_3(\boldsymbol{r_2})\rangle \\ \langle S_1(\boldsymbol{r_1})S_0(\boldsymbol{r_2})\rangle & \langle S_1(\boldsymbol{r_1})S_1(\boldsymbol{r_2})\rangle & \langle S_1(\boldsymbol{r_1})S_2(\boldsymbol{r_2})\rangle & \langle S_1(\boldsymbol{r_1})S_3(\boldsymbol{r_2})\rangle \\ \langle S_2(\boldsymbol{r_1})S_0(\boldsymbol{r_2})\rangle & \langle S_2(\boldsymbol{r_1})S_1(\boldsymbol{r_2})\rangle & \langle S_2(\boldsymbol{r_1})S_2(\boldsymbol{r_2})\rangle & \langle S_2(\boldsymbol{r_1})S_3(\boldsymbol{r_2})\rangle \\ \langle S_3(\boldsymbol{r_1})S_0(\boldsymbol{r_2})\rangle & \langle S_3(\boldsymbol{r_1})S_1(\boldsymbol{r_2})\rangle & \langle S_3(\boldsymbol{r_1})S_2(\boldsymbol{r_2})\rangle & \langle S_3(\boldsymbol{r_1})S_3(\boldsymbol{r_2})\rangle \end{pmatrix}, \quad (2.26)$$

where $\langle\ \rangle$ represents the ensemble average.

We use the two-point correlation of SPs to estimate the correlation of the Poincaré vector to access the spatial polarization dynamics. For this purpose, the normalized polarization correlation function is expressed [280] as

$$\gamma_p(\boldsymbol{r_1},\boldsymbol{r_2}) = \frac{\langle \boldsymbol{S}(\boldsymbol{r_1}).\boldsymbol{S}(\boldsymbol{r_2})\rangle}{\langle S_0(\boldsymbol{r_1})S_0(\boldsymbol{r_2})\rangle},$$

$$= \frac{\langle S_1(\boldsymbol{r_1})S_1(\boldsymbol{r_2})\rangle + \langle S_2(\boldsymbol{r_1})S_2(\boldsymbol{r_2})\rangle + \langle S_3(\boldsymbol{r_1})S_3(\boldsymbol{r_2})\rangle}{\langle S_0(\boldsymbol{r_1})S_0(\boldsymbol{r_2})\rangle},$$

$$= \frac{C_{11}(\boldsymbol{r_1},\boldsymbol{r_2}) + C_{22}(\boldsymbol{r_1},\boldsymbol{r_2}) + C_{33}(\boldsymbol{r_1},\boldsymbol{r_2})}{C_{00}(\boldsymbol{r_1},\boldsymbol{r_2})}. \quad (2.27)$$

Hence, diagonal elements of the two-point Stokes correlation matrix in Eq. (2.26) are sufficient to characterize the spatial polarization dynamics. The correlation of the Poincaré vector in Eq. (2.27) measures the similarity of the SOPs at the spatial points $\boldsymbol{r_1}$ and $\boldsymbol{r_2}$. The denominator in Eq. (2.27) is used to normalize the correlation function to ensure that the maximum value $\gamma_p(\max)$ is one, and $-1 \le \gamma_p(\boldsymbol{r_1},\boldsymbol{r_2}) \le 1$. Upper limit of γ_p correspond to the same SOPs at points $\boldsymbol{r_1}$ and $\boldsymbol{r_2}$, whereas a lower limit of γ_p correspond to mutually orthogonal SOPs at points $\boldsymbol{r_1}$ and $\boldsymbol{r_2}$.

Further, for the random field obeying Gaussian statistics, the second-order correlations of Eq. (2.26) are expressed as a sum of products of first-order correlations by applying the moment theorem [223,285]. Specifically,

$$C_{mn}(\boldsymbol{r_1},\boldsymbol{r_2}) = \sum_{a,b}\sum_{c,d} \sigma_{ab}^{m}\sigma_{cd}^{n} \left\langle U_a^*(\boldsymbol{r_1})U_b(\boldsymbol{r_1})U_c^*(\boldsymbol{r_2})U_d(\boldsymbol{r_2}\right\rangle$$

$$= \sum_{a,b}\sum_{c,d} \sigma_{ab}^{m}\sigma_{cd}^{n} \left[\left\langle U_a^*(\boldsymbol{r_1})U_b(\boldsymbol{r_1})\right\rangle \left\langle U_d^*(\boldsymbol{r_2})U_c(\boldsymbol{r_2})\right\rangle^* + \left\langle U_a^*(\boldsymbol{r_1})U_d(\boldsymbol{r_2})\right\rangle \left\langle U_b^*(\boldsymbol{r_1})U_c(\boldsymbol{r_2})\right\rangle^* \right],$$

$$= \sum_{a,b}\sum_{c,d} \sigma_{ab}^{m}\sigma_{cd}^{n} \left[W_{ab}(\boldsymbol{r_1},\boldsymbol{r_1})W_{dc}^*(\boldsymbol{r_2},\boldsymbol{r_2}) + W_{ad}(\boldsymbol{r_1},\boldsymbol{r_2})W_{bc}^*(\boldsymbol{r_1},\boldsymbol{r_2}) \right]. \tag{2.28}$$

For a time-frozen polarization speckle, the ensemble average is supplanted by the spatial average, considering spatial stationarity and ergodicity [225,286]. Due to the assumption of stationarity in space and considering $\boldsymbol{r_1} = \boldsymbol{r}, \boldsymbol{r_2} = \boldsymbol{r} + \boldsymbol{\Delta r}$, the two-point correlation of the SPs depends only on the difference in the spatial coordinates $\boldsymbol{\Delta r} = \boldsymbol{r_2} - \boldsymbol{r_1}$, i.e. $C_{mn}(\boldsymbol{r_1},\boldsymbol{r_2}) = C_{mn}(\boldsymbol{\Delta r})$.

The diagonal elements of Eq. (2.27) are represented as

$$C_{00}(\boldsymbol{\Delta r}) = \sum_{a,b}\sum_{c,d} \sigma_{ab}^{0}\sigma_{cd}^{0} \left[W_{ab}(0)W_{dc}^*(0) + W_{ad}(\boldsymbol{\Delta r})W_{bc}^*(\boldsymbol{\Delta r}) \right],$$

$$\begin{aligned} &= \sigma_{xx}^{0}\sigma_{xx}^{0} \left[W_{xx}(0)W_{xx}^*(0) + W_{xx}(\boldsymbol{\Delta r})W_{xx}^*(\boldsymbol{\Delta r}) \right] + \sigma_{xx}^{0}\sigma_{yy}^{0} \left[W_{xx}(0)W_{yy}^*(0) + W_{xy}(\boldsymbol{\Delta r})W_{xy}^*(\boldsymbol{\Delta r}) \right] \\ &+ \sigma_{yy}^{0}\sigma_{xx}^{0} \left[W_{yy}(0)W_{xx}^*(0) + W_{yx}(\boldsymbol{\Delta r})W_{yx}^*(\boldsymbol{\Delta r}) \right] + \sigma_{yy}^{0}\sigma_{yy}^{0} \left[W_{yy}(0)W_{yy}^*(0) + W_{yy}(\boldsymbol{\Delta r})W_{yy}^*(\boldsymbol{\Delta r}) \right], \end{aligned}$$

$$= \left|W_{xx}(0) + W_{yy}(0)\right|^2 + \left|W_{xx}(\boldsymbol{\Delta r})\right|^2 + \left|W_{xy}(\boldsymbol{\Delta r})\right|^2 + \left|W_{yx}(\boldsymbol{\Delta r})\right|^2 + \left|W_{yy}(\boldsymbol{\Delta r})\right|^2, \tag{2.29}$$

where, $W_{ab}(0)=\left\langle U_a^*(\boldsymbol{r})U_b(\boldsymbol{r})\right\rangle$, represents same point correlation, i.e., $\boldsymbol{r_1}=\boldsymbol{r}$ and $\boldsymbol{r_2}=\boldsymbol{r}$, and angular bracket $\langle\ \rangle$ represents the spatial average. The two-point field correlation of the random field is represented as, $W_{ab}(\boldsymbol{\Delta r})=\left\langle U_a^*(\boldsymbol{r})U_b(\boldsymbol{r}+\boldsymbol{\Delta r})\right\rangle$.

Performing similar calculations, we obtain,

$$C_{11}(\boldsymbol{\Delta r})=\left|W_{xx}(0)-W_{yy}(0)\right|^2+\left|W_{xx}(\boldsymbol{\Delta r})\right|^2-\left|W_{xy}(\boldsymbol{\Delta r})\right|^2-\left|W_{yx}(\boldsymbol{\Delta r})\right|^2+\left|W_{yy}(\boldsymbol{\Delta r})\right|^2, \tag{2.30}$$

$$C_{22}(\boldsymbol{\Delta r})=2\left|W_{xy}(0)\right|^2+2W_{xy}^2(0)+2\,\mathrm{Re}\left[W_{xx}(\boldsymbol{\Delta r})W_{yy}^*(\boldsymbol{\Delta r})+W_{xy}(\boldsymbol{\Delta r})W_{yx}^*(\boldsymbol{\Delta r})\right], \tag{2.31}$$

$$C_{33}(\boldsymbol{\Delta r})=2\left|W_{xy}(0)\right|^2-2W_{xy}^2(0)+2\,\mathrm{Re}\left[W_{xx}(\boldsymbol{\Delta r})W_{yy}^*(\boldsymbol{\Delta r})-W_{xy}(\boldsymbol{\Delta r})W_{yx}^*(\boldsymbol{\Delta r})\right]. \tag{2.32}$$

Addition of three diagonal elements $C_{11}(\boldsymbol{\Delta r}),C_{22}(\boldsymbol{\Delta r}),C_{33}(\boldsymbol{\Delta r})$ is

$$\begin{aligned}C_{11}(\boldsymbol{\Delta r})+C_{22}(\boldsymbol{\Delta r})+C_{33}(\boldsymbol{\Delta r})&=\left|W_{xx}(0)-W_{yy}(0)\right|^2+4\left|W_{xy}(0)\right|^2+\left|W_{xx}(\boldsymbol{\Delta r})\right|^2+\left|W_{yy}(\boldsymbol{\Delta r})\right|^2\\&-\left|W_{xy}(\boldsymbol{\Delta r})\right|^2-\left|W_{yx}(\boldsymbol{\Delta r})\right|^2+4\,\mathrm{Re}\left(W_{xx}(\boldsymbol{\Delta r})W_{yy}^*(\boldsymbol{\Delta r})\right).\end{aligned} \tag{2.33}$$

Substituting Eq. (2.29) and (2.33) into Eq. (2.27) provides

$$\gamma_p(\boldsymbol{\Delta r})=\frac{\begin{aligned}&\left|W_{xx}(0)-W_{yy}(0)\right|^2+4\left|W_{xy}(0)\right|^2+\left|W_{xx}(\boldsymbol{\Delta r})\right|^2+\left|W_{yy}(\boldsymbol{\Delta r})\right|^2-\left|W_{xy}(\boldsymbol{\Delta r})\right|^2-\left|W_{yx}(\boldsymbol{\Delta r})\right|^2\\&+4\,\mathrm{Re}\left(W_{xx}(\boldsymbol{\Delta r})W_{yy}^*(\boldsymbol{\Delta r})\right)\end{aligned}}{\begin{aligned}&=\left|W_{xx}(0)+W_{yy}(0)\right|^2+\left|W_{xx}(\boldsymbol{\Delta r})\right|^2+\left|W_{xy}(\boldsymbol{\Delta r})\right|^2+\left|W_{yx}(\boldsymbol{\Delta r})\right|^2+\left|W_{yy}(\boldsymbol{\Delta r})\right|^2,\end{aligned}} \tag{2.34}$$

This relation in Eq. (2.34) was related to the three statistical parameters, used for the characterization of spatial polarization dynamics. These three parameters are described as follows:

The spatial degree of coherence for spatially fluctuating electromagnetic field is defined as

$$\gamma^2_{EM\,(Space)}(\boldsymbol{\Delta r}) = \frac{\left|W_{xx}(\boldsymbol{\Delta r})\right|^2 + \left|W_{xy}(\boldsymbol{\Delta r})\right|^2 + \left|W_{yx}(\boldsymbol{\Delta r})\right|^2 + \left|W_{yy}(\boldsymbol{\Delta r})\right|^2}{\left|W_{xx}(0) + W_{yy}(0)\right|^2}, \tag{2.35}$$

In addition, we consider another quantity corresponds to the fringe visibility spatially averaged over the area of stationarity as

$$\gamma^2_{W}(\boldsymbol{\Delta r}) = \frac{\left|W_{xx}(\boldsymbol{\Delta r}) + W_{yy}(\boldsymbol{\Delta r})\right|^2}{\left|W_{xx}(0) + W_{yy}(0)\right|^2}, \tag{2.36}$$

Also, we used the spatial degree of polarization (SDOP) of the spatially fluctuating field as discussed in Eq. (2.5) and represented it in terms of single-point correlation of random field as,

$$P_s{}^2(0) = \frac{\left|W_{xx}(0) - W_{yy}(0)\right|^2 + 4\left|W_{xy}(0)\right|^2}{\left|W_{xx}(0) + W_{yy}(0)\right|^2}. \tag{2.37}$$

Substituting Eqs. (2.35)-(2.37), in Eq. (2.34), the right-hand-side of Eq. (2.34) is transformed as

$$\gamma_p(\boldsymbol{\Delta r}) = \frac{S_0^2(0)\left[P_s{}^2(0) - \gamma^2_{EM\,(Space)}(\boldsymbol{\Delta r}) + 2\left|\gamma_w(\boldsymbol{\Delta r})\right|^2\right]}{S_0^2(0)\left[1 + \gamma^2_{EM\,(Space)}(\boldsymbol{\Delta r})\right]},$$

$$= \frac{\left[P_s{}^2(0) - \gamma^2_{EM\,(Space)}(\boldsymbol{\Delta r}) + 2\left|\gamma_w(\boldsymbol{\Delta r})\right|^2\right]}{\left[1 + \gamma^2_{EM\,(Space)}(\boldsymbol{\Delta r})\right]}. \tag{2.38}$$

The SDOP, as represented in Eq. (2.37), can be used to classify the laser speckle into spatially fully polarized, partially polarized, and unpolarized light fields. Value of the

spatial DOP lies between $0 \le P_s(0) \le 1.$ The SDOP is 1 for a spatially fully polarized field, 0 for a spatially unpolarized field, and between 0 and 1 for a spatially partially polarized light field.

For a strictly spatially stationary and ergodic field, no correlation exists between the electric field as Δr approaches infinity, hence $\gamma_{EM(Space)}(\Delta r) \to 0, |\gamma_W(\Delta r)| \to 0$ and therefore, $\gamma_p(\Delta r) \to P_s{}^2(0),$ This implies that polarization states have a certain level of similarity regardless of spatially apart points in a partially polarized field.

Further, there is no significant variation of SOP throughout the random field for a spatially fully polarized light. However, the spatially partially polarized field experiences an appreciable SOP fluctuation. When the SOP fluctuation in space occurs in a completely random manner such that over a long length scale no preferred SOP exists, such field is termed a spatially unpolarized light field. However, there is a certain small distance over which no significant change in SOP fluctuation occurs. Therefore, the spatially unpolarized light can be treated as polarized light within this small distance. A concept of spatial polarization length specifies this length scale during which the SOP of the fluctuating field stays unaltered. Mathematically, the spatial polarization length is defined as the length at which $\gamma_p(\Delta r)$ decreases to half of its greatest worth as prescribed in Ref. [280].

2.3.2 Experimental setup

To test the viability of the proposed technique, we designed an experimental setup to create polarization speckles in a controlled fashion and non-interferometrically measure the SOP of the polarization speckle as shown in Fig. 2.8. The experimental setup consists of two major sections, i.e. part I and part II. Part I uses a triangular Sagnac geometry to synthesize the polarization speckle with different statistics by controlling the spatial

separation of the orthogonal polarization components. Part II represents the measurement of the SPs.

A detail of the experimental method is as follows. A spatially filtered vertically polarized light of wavelength 632.8 nm from a He-Ne laser is converted to a diagonally polarized light by orienting a half-wave plate (HWP) at 22.5^{o} with respect to the vertical direction. The diagonally polarized beam enters a triangular Sagnac geometry composed of a polarization beam splitter and mirrors M1 and M2. This geometry splits the diagonally polarized beam into two counter-propagating orthogonally polarized components. It makes their images on the ground glass (GG) plane by a lens L1 of focal length 250 mm. This scheme makes duplicate images of circular aperture (CA) on the GG as outlined in Fig. 2.8 and described in detail in Fig. 2.9. Mirrors M1, and M2 provide tuneable tilts to control the spatial separation of two orthogonally polarized images of the CA on the GG. The overlapping portion of the CA on the GG controls the spatial polarization distribution and statistics of the speckle. Scattering of the light beam from the GG scrambles the spatial polarization structure and creates a polarization speckle. This GG is placed at the front focal plane of lens L2 with a focal length of 250 mm, and a speckle pattern is recorded by a CCD placed at the back focal plane of L2. The recorded speckle patterns are created due to the superposition of the two orthogonally polarized scattered light beams. The CCD camera is pco.pixelfly with a dynamic range of 14-bit, resolution of 1024 x1392 pixels, and pixel pitch of 6.45µm.

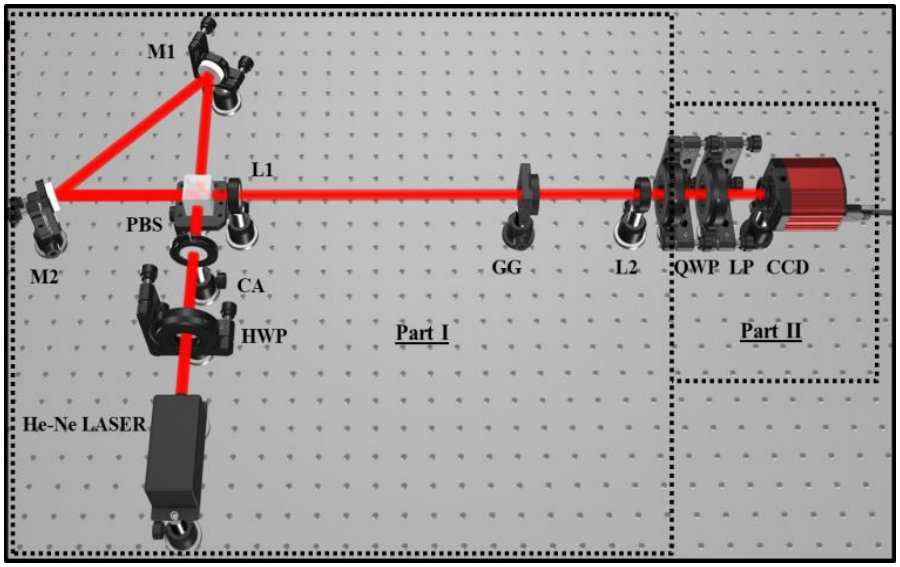

Fig. 2.8 Experimental setup for the synthesis of a time-frozen polarization speckle and SPs measurement. Laser: He-Ne laser; HWP: Half-wave plate; CA: Circular Aperture; PBS: Polarization Beam Splitter; M1, M2: Mirrors; L1, L2: Lenses; GG: Ground glass; QWP: Quarter-wave plate; LP: Linear polarizer; CCD: Charge-coupled device.

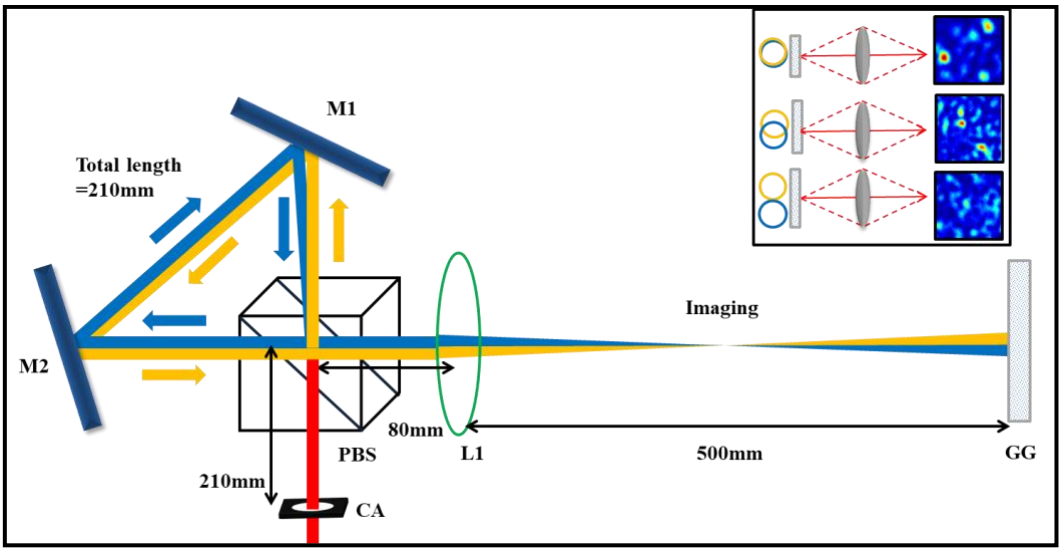

Fig. 2.9 Triangular Sagnac geometry is used to separate two counter-propagating orthogonally polarized components and their images on the GG plane. Yellow and blue colors represent two orthogonally polarized beams after a split from the PBS. A red color represents incident diagonally polarized light. The inset shows three different configurations of the orthogonal polarization components overlap to synthesize the polarization speckle.

Non-interferometric measurement of SPs is realized by capturing different intensities for different orientations of a linear polarizer (LP) and a quarter-wave plate (QWP). The SPs are extracted from the measured intensity patterns [119] as

$$\begin{aligned} S_0(\boldsymbol{r}) &= I(\boldsymbol{r},0^\circ,0^\circ) + I(\boldsymbol{r},90^\circ,0^\circ), \\ S_1(\boldsymbol{r}) &= I(\boldsymbol{r},0^\circ,0^\circ) - I(\boldsymbol{r},90^\circ,0^\circ), \\ S_2(\boldsymbol{r}) &= 2I(\boldsymbol{r},45^\circ,0^\circ) - S_0(\boldsymbol{r}), \\ S_3(\boldsymbol{r}) &= S_0(\boldsymbol{r}) - 2I(\boldsymbol{r},45^\circ,90^\circ), \end{aligned} \tag{2.39}$$

where $I(\boldsymbol{r},\theta,\varphi)$ is the intensity, θ refers to the LP angle, and φ refers to the phase of the QWP.

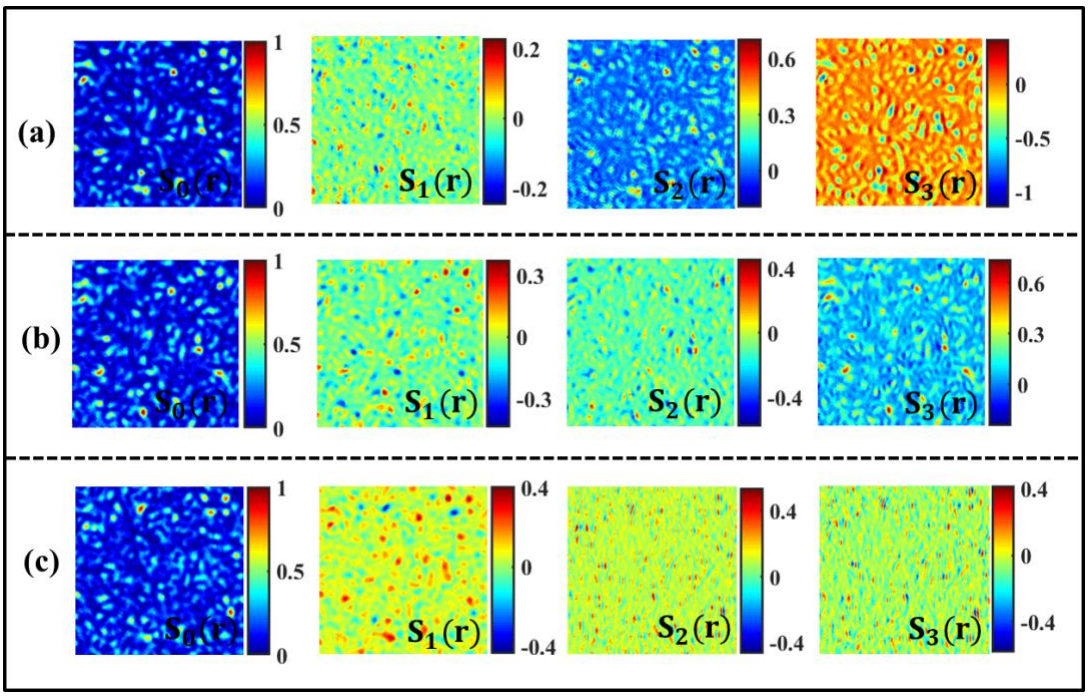

Fig. 2.10 Panels (a)-(c) represents experimentally measured SPs for three different cases of the polarization speckle (a) full overlap; (b) half overlap; (c) full separation.

The SPs are used to determine the two-point correlation and the spatial polarization dynamics of the polarization speckle as described by Eq. (2.27). From the experimentally measured SPs, digital evaluation of two-point Stokes correlations is obtained by spatial averaging under the assumption of spatial stationarity and ergodicity. This process is

executed by taking 1000 × 1000 pixels of the recorded SPs and 2D scanning of $S_m^{\kappa}(x,y)$ where *x* and *y* are spatial pixel coordinates which are taken as 100x100 pixels, providing 900x900 random realizations for the spatial averaging. $S_m^{\kappa}(x,y)$ represents one realization of the SP of the scattered field. Here, the two-point Stokes correlation for different realizations of random patterns is represented as $\sum_{\kappa=1}^{900^2} S_m^{\kappa}(x,y) S_n^{\kappa}(0,0)$, where $S_n^{\kappa}(0,0)$ denotes the centre pixel of the selected window of the speckle pattern. Window $S_m^{\kappa}(x,y)$ arises due to pixel-by-pixel scanning of the matrix $S_m^{\kappa}(x,y)$ over the experimentally recorded SPs. The two-point Stokes correlations are digitally obtained to measure the normalized polarization correlation function $\gamma_p(\Delta \boldsymbol{r})$ of polarization speckles as explained in Eq. (2.27).

2.3.3 Simulation and experimental results

The illuminating beam size of the CA on the GG is 4 mm. By controlling the separation of the two orthogonally polarized light beams impinging on the GG, three different cases of polarization speckle are generated with three different spatial polarization fluctuations as shown in Eq. (2.37). Simulation of the polarization speckle is realized by numerically generating two coherent orthogonally polarized light fields with a size of 4 mm and 632.8 nm wavelengths. These orthogonal polarization components with different separations propagate through the GG as shown in Fig. 2.9. The GG inserts uniform random phase distribution in the range of $[-\pi,\pi]$ in the orthogonal polarization components which are digitally propagated from source to observation plane by a discrete fast Fourier transform. Three different source structures are created by controlling the separation between two orthogonally polarized lights on the GG. Hence, a combination of orthogonal polarization states creates a polarization speckle at the observation plane. The SPs of the random field

are used to compute the Poincaré vector correlations and the normalized polarization correlation function to evaluate the polarization dynamics of polarization speckles.

A set of four experimentally measured SPs for three different cases of polarization speckles is shown in Fig. 2.10. The first set represented by Fig. 2.10(a) presents the results of the SPs for a fully overlapping case wherein both orthogonal polarization components propagate through a common portion of the GG. Fig. 2.10(b) represents the SPs for a spatially partially polarized (half overlap) case where half portion of the orthogonally polarized sources get a common random phase from the GG and the remaining portions of the orthogonal polarization components get different and independent random phase values. A panel in Fig. 2.10(c) represent the SPs for a fully separated case where the orthogonal polarization components get completely independent random phases from the GG. From the experimentally measured SPs, mapping of the Poincaré vector on the Poincaré sphere shows the random spread of the SPs over the Poincaré sphere. Hence, mapping of full-field on the Poincaré sphere is a very arduous task to distinguish the different illumination conditions of the light beam falling on the GG and observe the spatial variations of the SOP. However, the impact of the spatial polarization fluctuations of the light field on the spatial variation of the SOP can be demonstrated by observing the correlation between the SPs at the spatial points to measure the normalized polarization correlation function, $\gamma_p(\boldsymbol{\Delta r})$, as explained in Eq. (2.27), (2.38).

Simulation and experimental results of the normalized polarization correlation function $\gamma_p(\boldsymbol{\Delta r})$ for three different overlapping of the CA images on the GG with are shown in Fig. 2.11. We see that with the increase in separation of two orthogonally polarized sources on the GG, the amount of spatial polarization variation increases. Simulation and

experimental results of profiles of $\gamma_p(\Delta \boldsymbol{r})$ are shown in Fig. 2.12 to depict the polarization correlation along the horizontal axis as we have stretched the orthogonally polarized sources in the horizontal axis. It is observed that as the separation between orthogonally polarized sources increases, the correlation along the horizontal axis decreases. A small deviation in the experimental results in comparison to the simulation could be due to experimental constraints like beam profile, optics, etc. We introduce the spatial polarization length to quantitatively measure the polarization fluctuation and this quantity is defined as the length at which $\gamma_p(\Delta \boldsymbol{r})$ drops to half of its maximum value. The polarization length for the half overlapping case is 45.15 μm and it is further reduced to 19.35 μm for the fully separated case. For the fully overlapping case $\gamma_p(\Delta \boldsymbol{r})$ only drops to 15% of its peak value $\gamma_p(0)$. Hence, the polarization length is large for the fully overlapping case.

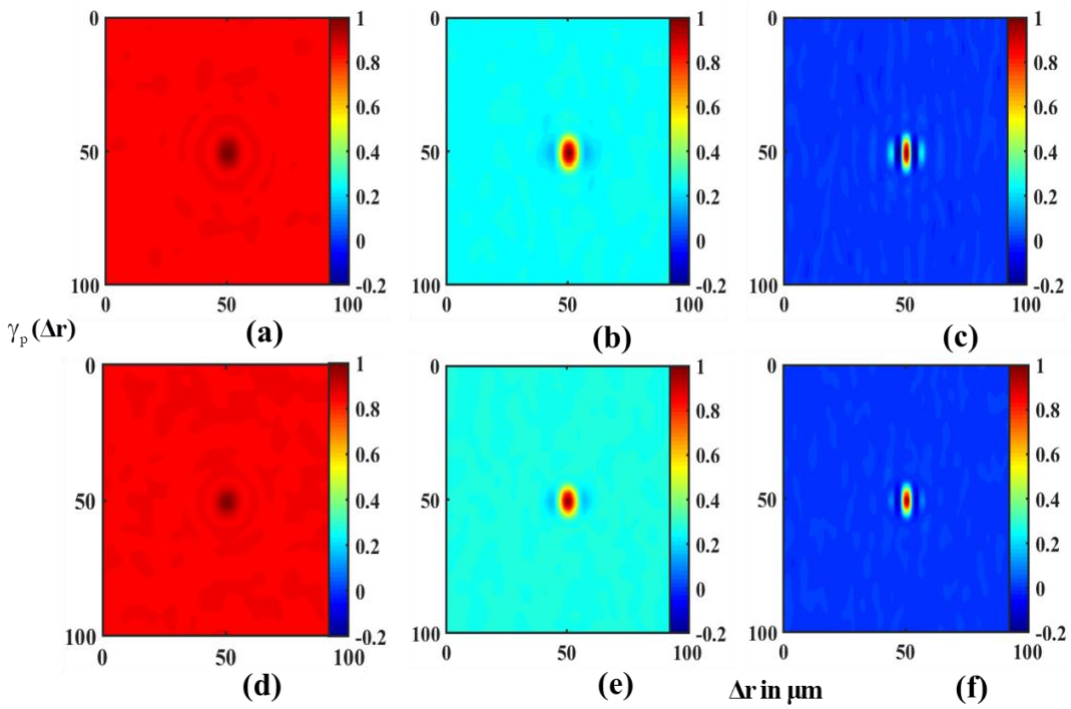

Fig. 2.11 Panels (a)-(c) and (d)-(f) represent simulation and experimental results of the distribution of normalized polarization correlation function $\gamma_p(\Delta r)$ for illuminating beam size 4mm and three different amounts of overlap (a, d) full overlap; (b, e) half overlap; (c, f) full separation. Pixel numbers are given on two axes.

An error parameter is also introduced to compare the experimental and simulation results.

The error parameter is given by, $Err = \frac{|experimental\ value\text{-}theoretical\ value|}{|theoretical\ value|} \times 100\%$.

For the fully overlapped case, the '*Err*' is 1.6%. Similarly, the '*Err*' for the half-overlapping and fully separated cases is 8.4%, and 2.4%, respectively.

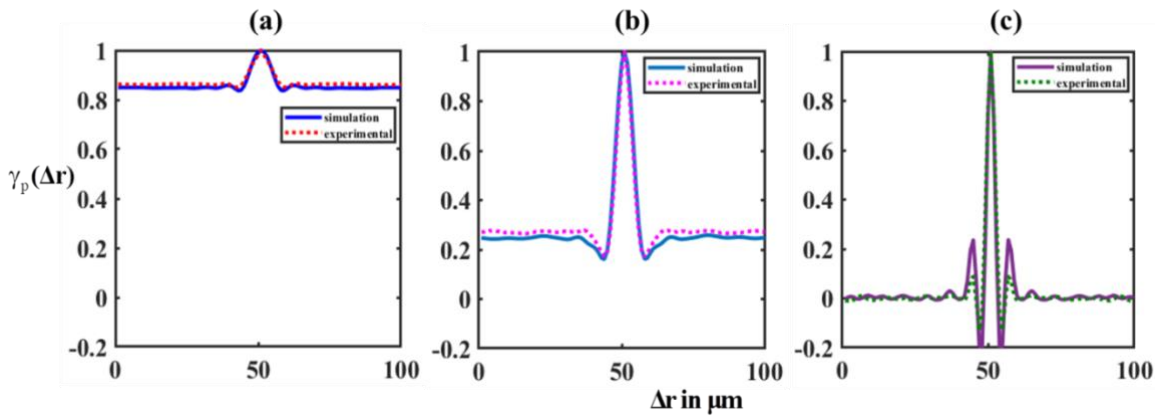

Fig. 2.12 Panels (a)-(c) represent profiles of simulation and experimental results of the normalized polarization correlation function $\gamma_p(\Delta r)$ along the horizontal axis for illuminating beam size 4mm and three different amounts of overlap (a) full overlap; (b) half overlap; (c) full separation. Pixel number (51, 51) represents the origin of the coordinate of $\gamma_p(\Delta r)$ at which $\Delta r = 0$.

2.4 Conclusion

In this chapter, we have proposed and experimentally demonstrated two novel techniques for the statistical characterization of polarization speckle. In the first technique, we utilize the concept of vMF distribution on the Poincaré sphere to study the spatial evolution of the polarization state of the polarization speckle fields. Here, we measured the SPs using a polarization interferometry setup and a relation between the SDOP and averaged NSPs with the spatial concentration parameter and spatial mean direction are established. Our method characterizes the SOP fluctuations of polarization speckle through the parameters $(P_s, \omega_s) \rightarrow (\kappa_s, \mu_s)$ and to couple it with Poincaré graphical method. In this thesis, we have explored the statistical insights of polarization speckle for fully coherent light sources. However, extending this statistical analysis to partially coherent light sources and extreme scattering conditions will require modifications to the vMF model, which will be considered in future work. In the second technique, we explore the correlations of the Poincaré vector using a two-point Stokes correlation to gain insight into the spatial

variation of polarization states fluctuation of polarization speckle. To demonstrate the feasibility of the proposed technique, we have presented simulation and experimental results for the three different types of polarization speckles. The expected outcome of this research spans across the domains of optics and photonics, encompassing applications such as the characterization of random fields, optical sensing, information about the scale of polarization speckle grain, and potential analogical applications in the field of quantum optics.